Pergamon

Cement and Concrete Research 32 (2002) 1407–1420

CEMENT AND CONCRETE RESEARCH

Stress and strain state of concrete during freezing and thawing cycles

Vesa Penttala*, Fahim Al-Neshawy

Department of Civil and Environmental Engineering, Building Materials Technology, Helsinki University of Technology, P.O. Box 2100, FIN-02015 HUT, Finland

Received 22 February 2001; accepted 12 March 2002

Abstract

The objective of this work is to calculate the pressures, stresses, and strains induced into moist concrete during freezing and thawing. The applied theory is based on thermodynamics and the linear theory of elasticity. If no additional salts are dissolved in the pore water the inputs needed in the theory are relative humidity and temperature measured in the sample chamber and inside concrete and evaporable water amount in the pore structure. Theoretical results were compared with the test results made with two concretes cured under water or at 96% relative humidity. One of the concretes was air entrained and in the comparison concrete no air-entraining agents were used. In the test cylinders cured under water the largest tensional stresses in freezing occurred on the surface of the test cylinders both in the axial and tangential direction. The largest tensional stress was 2.2 MPa, both in air-entrained and in non air-entrained concretes. The largest tensional stresses in the warming phase took place at the end of the thawing period when the chamber temperature was around +5 °C. Then the maximum tension occurred in the middle of the concrete cylinder in the axial direction of the cylinder. This maximum tensional stress was over 2.5 MPa in the air-entrained concrete cured in the relative humidity of 96%. The thermodynamic pumping effect at the end of the thawing phase in every cycle can increase the pore water amount remarkably if free water or moisture is available on the surface of the structure or in the environment vapor. The thermodynamic pumping effect seems to be remarkably greater and more dangerous in air-entrained concretes.

Keywords: Concrete; Freezing and Thawing; Modeling; Stresses; Strains

1. Introduction

Modelling of concrete behavior under different loading conditions is often based on crude assumptions and semi-scientific dimensioning theories. The dimensioning rules are usually very simplified and take into consideration only one or two main features of the material behavior. This state of contemporary practice is considered justified due to the very complicated material features of concrete. Concrete can be considered as one of the most nonhomogeneous and demanding engineering materials used by mankind. This man-made artificial stone consists of aggregates having a wide dimensional range from submicron particles to several centimeters. Aggregate particles are usually surrounded by a transition zone differing from the bulk matrix of hydrated and partially hydrated cement paste, which is highly porous. Void dimensions range from nanometer-sized gel pores of calcium silicate hydrates to micrometer-sized capillary pores and larger pores of several millimeters covering a dimensional range of over six orders of magnitude. The pore system is partially filled with water.

The glue phase of calcium silicate hydrates is also very complicated, comprising of amorphous and crystalline phases. One of the general features of concrete is the large number of cracks that are induced into it in normal climatic conditions. The defects are partly due to shrinkage tensions caused by the contraction of the matrix gel and by moisture and temperature gradients between different parts of the concrete structure.

The freezing and thawing durability of concrete is of utmost importance in countries having subzero temperature conditions. For example, nearly one third of all concrete poured in Nordic countries should possess adequate freezing and thawing resistance. However, the stresses and strains in concrete caused by freezing and thawing loads are nearly totally unknown and the building regulations for the pro-

* Corresponding author. Tel.: +358-9-451-3770; fax: +358-9-451-3826.

E-mail address: vesa.penttala@hut.fi (V. Penttala).

0008-8846/02/$ – see front matter
PII: S0008-8846(02)00785-8

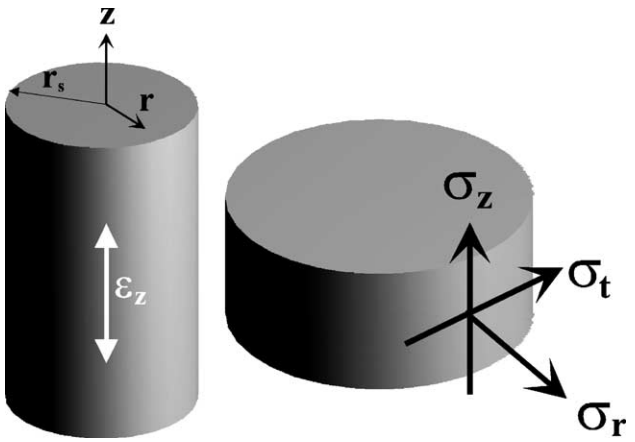

Fig. 1. Test cylinder and coordinate, stress, and strain notations.

duction of freezing durable concrete are based on standardized test procedures and indirect production rules. This paper is an attempt to derive the pressures, stresses, and strains induced into concrete during freezing and thawing of the pore water. The paper is based on general laws of nature of which thermodynamics is one of the most powerful. The stresses and strains in the freezing structure, e.g., in this situation concrete cylinder, are calculated according to the linear theory of elasticity.

2. Literature review

The first one to study freezing and thawing of concrete paste was T.C. Powers [1,2] together with his coworkers T.L. Brownyard and R.A. Helmuth [3–5]. Powers presented a theory of hydraulic pressure in which the pore water in the largest pores freezes first during cooling and only after the smaller pores have been frozen would the expansion be hindered causing large hydraulic pressures and subsequent paste destruction.

Powers and his coworkers also observed another freezing mechanism: the growth of the bodies of ice in the capillary cavities or air voids by diffusion of water from the nanometer-sized gel pores. However, they assumed that this mechanism always caused expansion in hardened Portland cement paste. Their experiments showed that empty air voids limit the hydraulic pressure and shorten the period during which ice in the cavities can increase. The closer these entrained air voids are to each other the more effective they are in controlling the two freezing mechanisms.

Everett [6] and Everett and Haynes [7] showed that ice in a larger pore could grow to a smaller, water-filled pore only when the interface between ice and the water in the connecting tube between the large and smaller pore would be curved. Due to this curvature a lower pressure would be induced into the smaller, unfrozen pore water, which would draw water from the smaller pores to the ice crystal until ice could not expand any more because of lack of space.

The third important theoretical impact on the freezing theories of porous solids was done by Litvan [8,10,11] and Sidebottom and Litvan [9]. According to Litvan's model, the surface forces of pores have an important effect during the freezing of pore liquid. These surface forces hinder ice crystal formation and the water layer situated a few molecular diameters from the surface remains structurally oriented during the freezing of rest of the pore water. Setzer [12] criticizes Litvan's assumptions of constant surface stresses in the adsorbed interface between vapor and the capillary condensed liquid where Litvan assumes a zero contact angle between the liquid meniscus and pore surface. Due to Litvan's simplified

Table 1
Composition and compressive strength data of the test concretes

Test concrete	K40A2	K40A5
Aggregates (kg/m^3) total	1902.6	1746.6
# 8–16 mm	513.7	506.5
# 5–10	399.5	366.8
# 2–5	228.3	174.6
# 1–2	171.2	157.2
# 0.5–1.2	190.3	174.7
# 0.1–0.6	209.3	192.1
# <0.125	190.3	174.7
Cement (kg/m^3)	281.1	365.8
Water (kg/m^3)	180.7	172.7
Air-entraining admixture (kg/m^3)	–	0.1
Compressive strength (MPa) 100-mm cubes	45.8	45.8

Table 2
Chemical composition and physical properties of cement CEM IIA 42,5R

Chemical composition (wt.%)	
CaO	60.7
SiO_2	20.5
Al_2O_3	5.0
Fe_2O_3	2.4
MgO	3.1
K_2O	0.80
Na_2O	0.85
SO_3	3.1
Loss of ignition (950 °C)	3.4
Physical properties	
Compressive strength (MPa)	
1 day	19.2
7 days	44.1
28 days	49.2
Specific area (Blaine) (m^2/kg)	470

Table 3
Pore data of the test concretes

Test concrete	Relative humidity [%]	Evaporable pore water volume [mm^3/cm^3 concrete]	Total pore volume [mm^3/cm^3 concrete]	Protective pore ratio
K40A2,RH100	100	148.4	160.2	0.09
K40A2,RH96	96	121.4	157.2	0.09
K40A5,RH100	100	133.1	180.8	0.23
K40A5,RH96	96	109.7	180.6	0.22

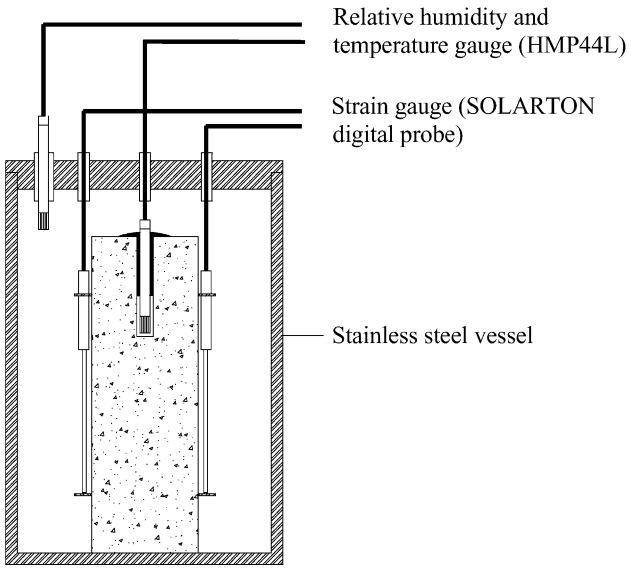

Fig. 2. Test arrangement in the freezing and thawing tests.

assumptions, for example, gel water could not freeze. Setzer presented a revised thermodynamic model based on Litvan's basic assumptions but taking into consideration the changes in surface stresses in the adsorbed water layer on the pore surface during the thickness changes of this adsorbed, structurally oriented water layer. A somewhat more refined literature review on the subject is presented in Refs. [13,14].

3. Pressures in pore water before and after freezing

Liquids in porous materials behave differently compared to bulk liquids. For instance, the triple point temperature and pressure in which all phases (vapor, liquid, and solid) of the liquid can exist simultaneously is changed. If the liquid is water and no ice is present in the pore system, water pressure in a porous material is governed by Kelvin's equation

$$p - p_0 = \frac{RT}{v_w} \ln\left(\frac{p_v}{p_{v0}}\right) \quad (1)$$

in which T is the ambient temperature presented in Kelvins, p is the pressure of water, p_0 denotes the reference pressure, which has been chosen as the atmospheric pressure 0.1 MPa. p_v is the vapor pressure in the pore system and $p_{v0} = p_{v0}(T, p_0)$ is the saturated vapor pressure of the liquid in the pressure p_0 at the ambient temperature. R is the gas constant 8.314 J/mol/K and v_w is the specific volume of the liquid. The relative humidity of the pore system ϕ equals p_v/p_{v0}, and if it is, for example, 0.85, the pressure of pore water $(p - p_0)$ is -22 MPa at 20 °C. This negative pressure effects only on evaporable water in concrete. In order to calculate its total effect on the cross section of the structure it must be multiplied by the ratio V_{evap}/V_{con} in which V_{evap} denotes evaporable water volume and V_{con}

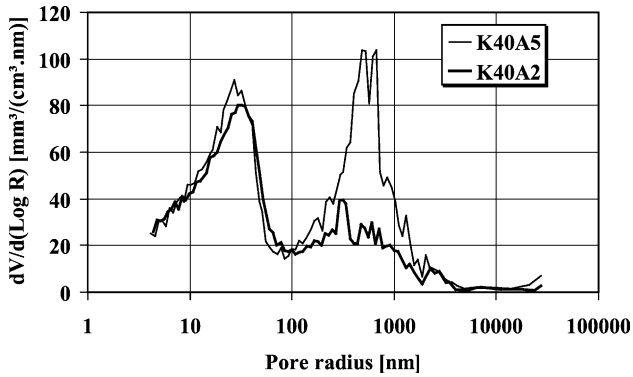

Fig. 3. Pore size distributions of the test mortars produced by mercury intrusion. The MIP tests were performed according to Ref. [18].

volume of concrete. For example, in concrete having a compressive strength of 40 MPa and cured at 85% relative humidity the evaporable water amount is around 110 mm^3/concrete cm^3. This can be calculated by weighing the concrete in air and under water before heating the sample to 105 °C. The pore water pressure calculated on the whole cross section in the middle part of 40 MPa concrete is roughly -2.4 MPa.

In the middle part of the concrete cross section negative water pressure causes compression in the structure and it is one of the reasons for the structural integrity and mechanical properties of concrete. If this negative pore pressure caused by pore water did not exist concrete would possess weaker strength properties and this would diminish the use of concrete as a load-bearing material. For example, Kelvin's equation explains why wet concrete

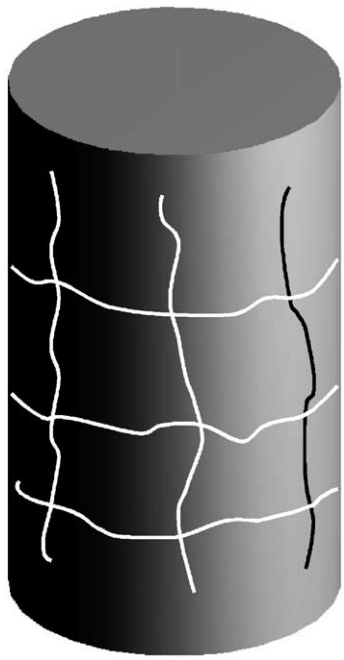

Fig. 4. Typical crack pattern in the test specimen after the freezing and thawing test.

has inferior mechanical properties compared to dry concrete. This physical phenomenon affects all microporous materials and, similarly, the strength of paper is mainly caused by the hydrogen bonds of the water molecules. If those water-induced forces would be lacking, paper would easily disintegrate to pulp mass.

When ice forms in the pore system of a porous material freezing-induced pressures are generated. Penttala [13,15] has derived a theory by which the liquid pressure can be calculated in a freezing porous material.

$$p - p_0 = \frac{RT}{v_i}\ln\left(\frac{p_v}{\gamma_w x_{unf} p_{v0}}\right) + \frac{\Delta h^\circ_{wi}}{v_i T_0}(T_0 - T) + \frac{1}{v_i}\int_{T_0}^{T}\int_{T_0}^{T}\frac{c^\circ_{pi} - c^\circ_{pw}}{T}\mathrm{d}T\mathrm{d}T \quad (2)$$

$$p - p_0 = \frac{\Delta h^\circ_{wi}}{(v_i - v_w)T_0}(T_0 - T) + \frac{1}{(v_i - v_w)}\int_{T_0}^{T}\int_{T_0}^{T}\frac{c^\circ_{pi} - c^\circ_{pw}}{T}\mathrm{d}T\mathrm{d}T \quad (3)$$

Eq. (2) represents the situation when ice is forming in a pore partially filled with gas and pore liquid while Eq. (3) gives pore pressures when the freezing pore is totally free of gas bubbles and all pores are filled with liquid. The latter situation is almost never valid when pore water first freezes due to self-desiccation and the quite large evaporation of water when the surface of concrete is in contact with air. Only when non air-entrained concrete freezes under water the pore structure can be totally filled with water when pore water first freezes. Therefore, Eq. (3) governs the freezing process only after freezing has commenced in so small pore

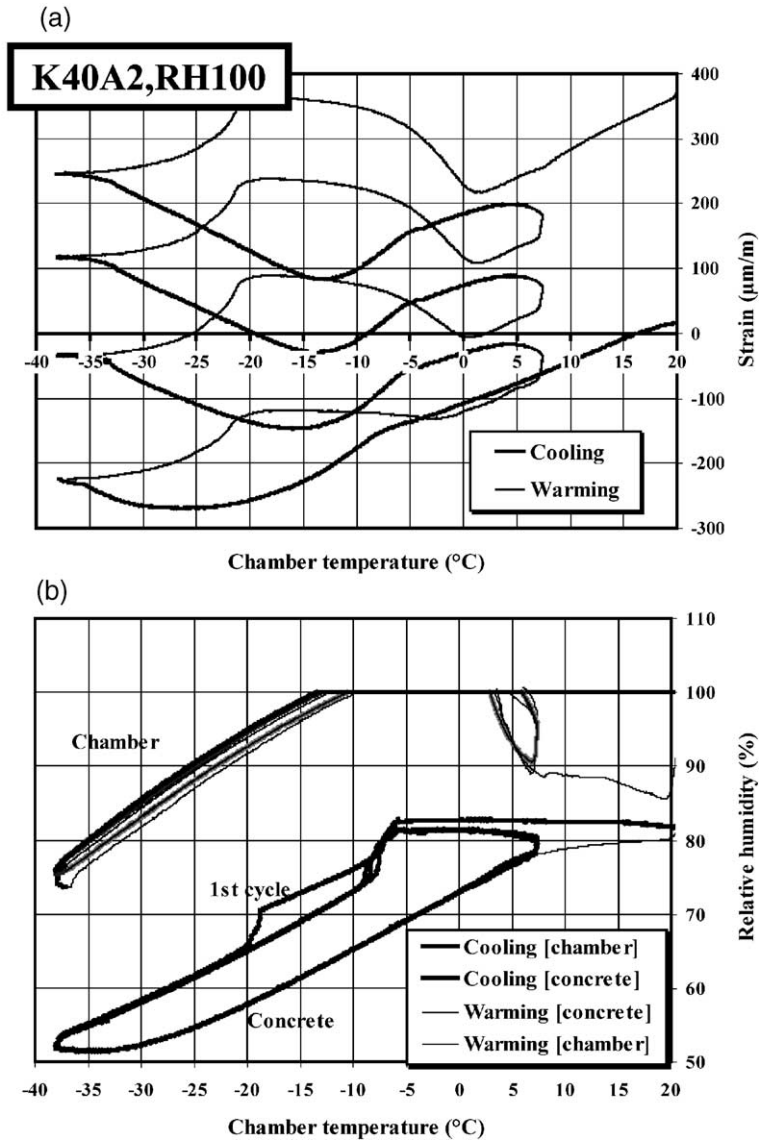

Fig. 5. Axial strain and relative humidity results of test concrete K40A2,RH100 cured under water.

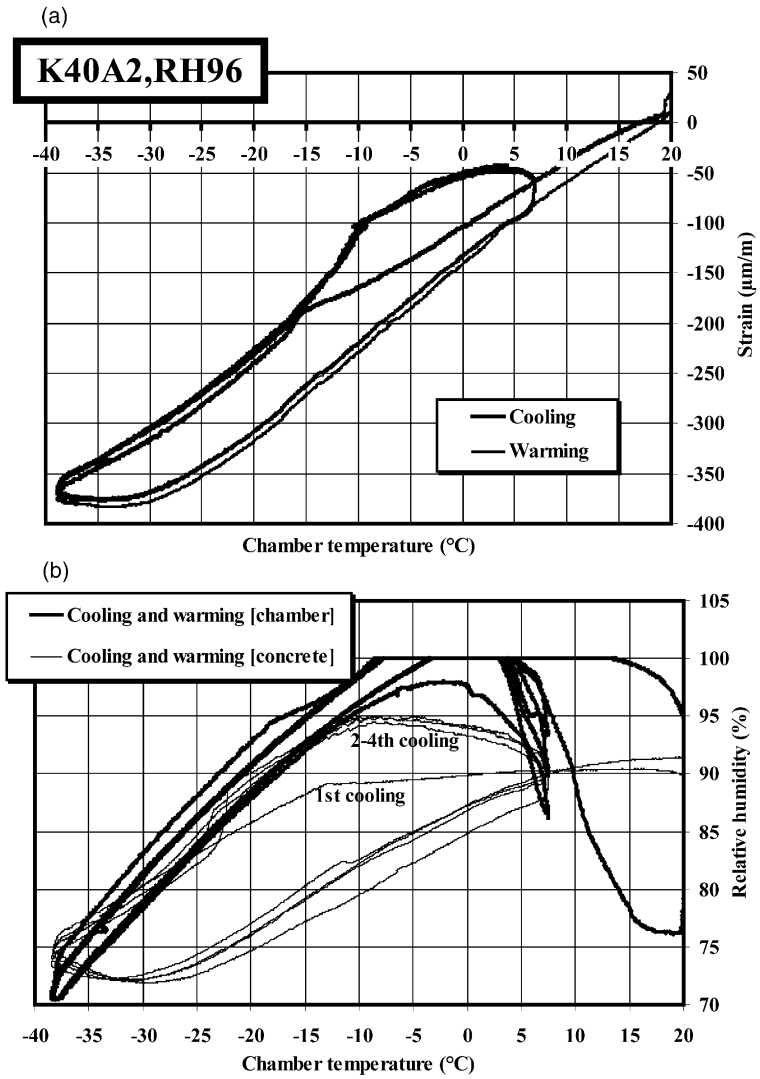

Fig. 6. Axial strain and relative humidity results of test concrete K40A2,RH96 preserved in relative humidity of 96%.

sizes that they are totally filled with liquid before freezing. Eq. (3) gives pore liquid pressures that are much larger compared to the values obtained by Eq. (2). Eq. (3) has been derived also by Brun et al. [16]. The following presentation is based on Eq. (2).

In the formulae Δh°_{wi} is the freezing heat of the liquid at the reference temperature T_0 and v_i is the specific volume of the solid phase of the liquid. If the pore liquid is water, the specific volume of ice is $v_i = 1.998 \times 10^{-5}$ m^3/mol, the specific volume of water is $v_w = 1.8 \times 10^{-5}$ m^3/mol, $T_0 = 273.15$ °K and $\Delta h^{\circ}_{wi} = 6.0 \times 10^3$ J/mol [17]. The specific heat capacities of ice and water, c°_{pi} and c°_{pw}, cannot be considered constant in the rather large temperature range in question and therefore the following equations will be used [16]

$$c^{\circ}_{pi}(T) = 38.052[1 + 373.7 \times 10^{-5}(T - T_0)] \quad (4)$$

$$c^{\circ}_{pw}(T) = 75.996[1 - 54.0 \times 10^{-5}(T - T_0)]. \quad (5)$$

The specific heat capacities of ice and water of Eqs. (4) and (5) are presented in joules per mole. When the c°_{p} formulae (4) and (5) are used in Eqs. (2) and (3) they have to be integrated numerically. The term x_{unf} denotes the mole fraction of pore water before freezing, and if no additional salts have been dissolved into the pore water $x_{unf} = 1$. The activity coefficient γ_w has the value of 1 in the case of an ideal solution in which both solvent and solute obey Raoult's law.

In order to calculate the pressures in the pore water by Eq. (2) only the relative humidity and temperature in the specific part of concrete structure must be known. All other terms in Eq. (2) are known thermodynamic properties. If additional salts are dissolved into the pore water the mole fraction of unfrozen pore water x_{unf} and activity coefficient γ_w must be known. To calculate the pressures induced into concrete due to freezing forces evaporable water volume must also be measured.

4. Stresses and strains in a cylindrical concrete specimen

The test cylinders were monitored so that relative humidity and temperature were measured in the middle of the test cylinder and in the test chamber. This enabled the calculation of the pore water pressures at the outer surface and in the middle of the test specimen by Eqs. (1) and (2) before and after the first freezing temperature during the cooling and warming cycles. The axial strain on the outer surface was measured by inductive length measuring gauges, which were calibrated by cooling and warming a steel cylinder having a known coefficient of temperature expansion. The coordinates, stress, and strain notations of the cylinder are presented in Fig. 1.

The derivation of the stress and strain formulae were done assuming that concrete obeyed the linear theory of elasticity and no cracks would exist or would be induced into the test specimen. This assumption is, of course, very theoretical as it is known that shrinkage cracks most certainly will be induced into the specimen prior to the freezing and thawing test and freezing loads will also cause additional crack formation at least in the test specimen cured in very moist environment. First, the stress and strain formulae for the freezing and thawing loads will be derived and, thereafter, the stresses and strains caused by the temperature differences between the outer and inner parts of the cylinder will be presented.

The stress state before and after freezing caused by the pore water pressure loads $p=p(r)$ can be calculated by equations

$$\sigma_r = \frac{E}{1+\nu}\left(\varepsilon_r + \frac{\nu}{1-2\nu}e\right) + p(r)\frac{V_{\text{evap}}}{V_{\text{con}}} \tag{6}$$

$$\sigma_t = \frac{E}{1+\nu}\left(\varepsilon_t + \frac{\nu}{1-2\nu}e\right) + p(r)\frac{V_{\text{evap}}}{V_{\text{con}}} \tag{7}$$

$$\sigma_z = \frac{E}{1+\nu}\left(\varepsilon_z + \frac{\nu}{1-2\nu}e\right) + p(r)\frac{V_{\text{evap}}}{V_{\text{con}}} \tag{8}$$

$$e = \varepsilon_r + \varepsilon_t + \varepsilon_z \tag{9}$$

$$\varepsilon_z = const.$$

As Poisson's coefficient ν of concrete, the value of 0.17 is used in the experimental part of the article. Because freezing and thawing pressures were calculated only at the outer surface and in the middle of the specimen, the pressure

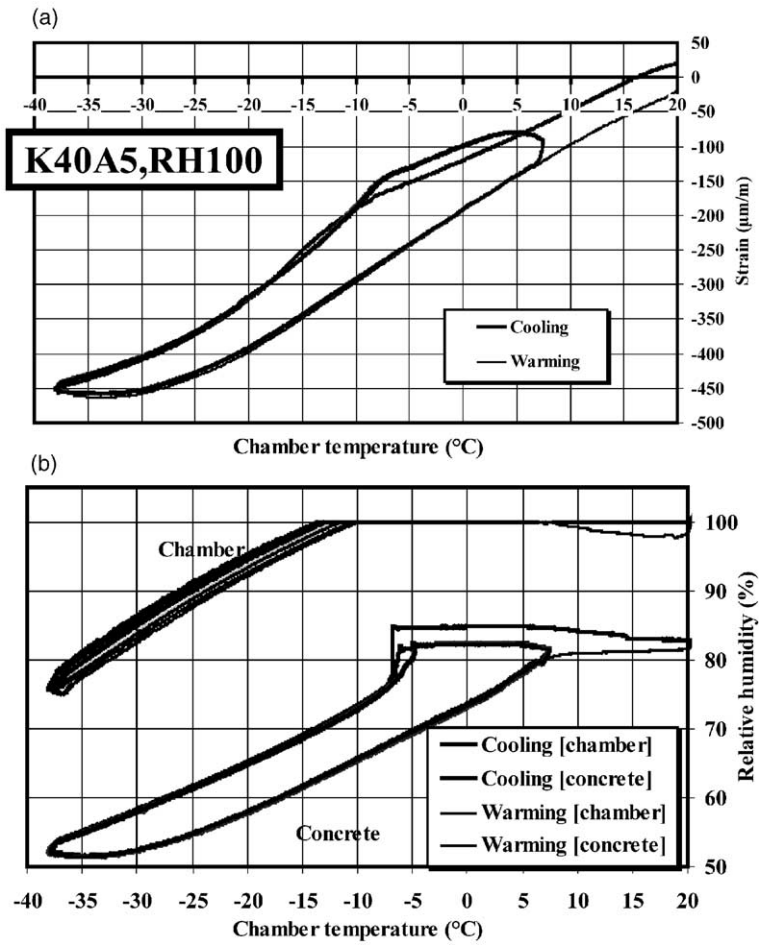

Fig. 7. Axial strain and relative humidity results of test concrete K40A5,RH100 cured under water.

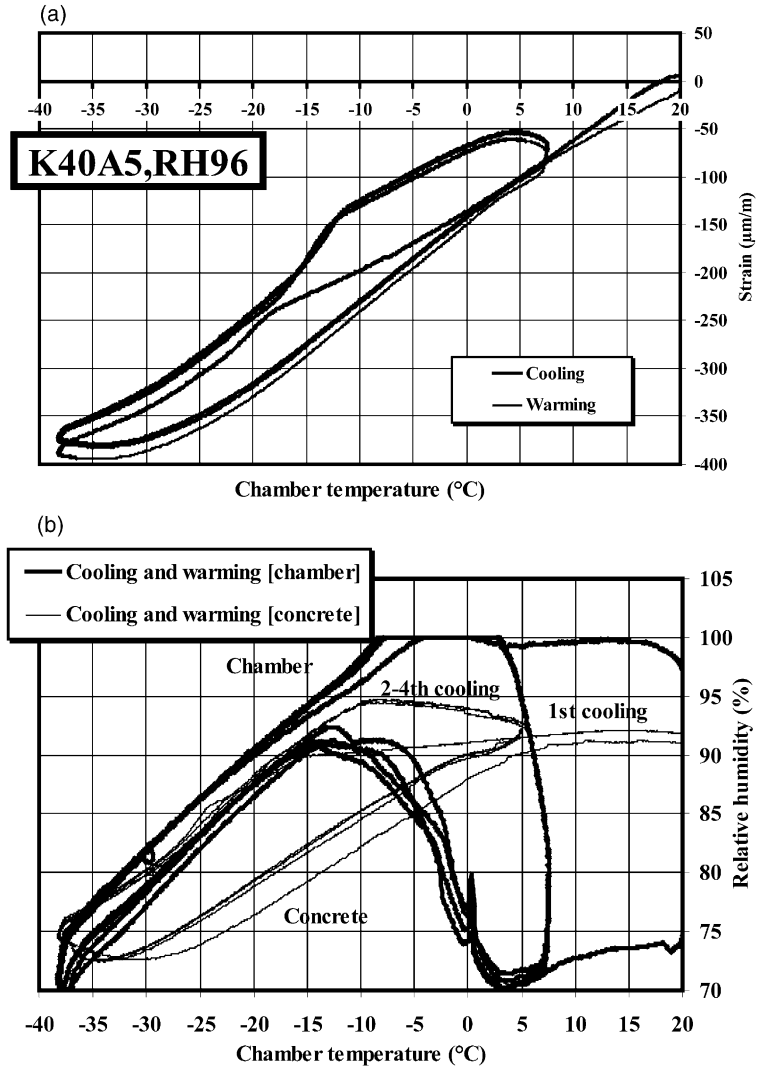

Fig. 8. Axial strain and relative humidity results of test concrete K40A5,RH96 preserved in relative humidity of 96%.

distribution of the pore water was assumed linear in the radial direction of the cylinder.

$$p(r) = p_{\mathrm{i}} + (p_{\mathrm{s}} - p_{\mathrm{i}})\frac{r}{r_{\mathrm{s}}} \tag{10}$$

in which p_{i} is the pressure in the middle of the cylinder calculated by Eq. (1) or (2), p_{s} is the pressure on the surface of the cylinder, and r_{s} is the radius of the cylinder. The equilibrium equation of the stress state is

$$\frac{\partial \sigma_r}{\partial r} + \frac{\sigma_r - \sigma_t}{r} = 0 \tag{11}$$

Inserting Eqs. (6)–(9) into Eq. (11) and taking into consideration equations

$$\varepsilon_r = \frac{\partial u}{\partial r} \quad \varepsilon_t = \frac{u}{r}$$

the following stress equations were derived

$$\sigma_r = \frac{V_{\mathrm{evap}}}{V_{\mathrm{con}}}(p_{\mathrm{i}} - p_{\mathrm{s}})\left[1 - \frac{2-\nu}{3(1-\nu)}\right]\left(1 - \frac{r}{r_{\mathrm{s}}}\right) \tag{12}$$

$$\sigma_t = \frac{V_{\mathrm{evap}}}{V_{\mathrm{con}}}\frac{(p_{\mathrm{i}} - p_{\mathrm{s}})}{(1-\nu)} \times \left[(1-\nu)\left(1 - \frac{r}{r_{\mathrm{s}}}\right) + \frac{1+\nu}{3}\left(1 + \frac{r}{r_{\mathrm{s}}}\right) - 1\right] \tag{13}$$

$$\sigma_z = \frac{V_{\mathrm{evap}}}{V_{\mathrm{con}}}(p_{\mathrm{i}} - p_{\mathrm{s}})\frac{1-2\nu}{1-\nu}\left(\frac{2}{3} - \frac{r}{r_{\mathrm{s}}}\right) \tag{14}$$

Strain in the outer surface in the direction of the z axis of the cylinder is

$$\varepsilon_z = \frac{1}{E_{\mathrm{c}}}[\sigma_z - \nu(\sigma_r + \sigma_t)] - \frac{1-2\nu}{E_{\mathrm{c}}}p(r)\frac{V_{\mathrm{evap}}}{V_{\mathrm{con}}} \tag{15}$$

E_c is the modulus of concrete, V_{evap} is the evaporable water volume in concrete volume V_{con}. The stresses caused by the temperature differences between outer surface and the inside of the concrete specimen are

$$\sigma_r = \frac{\alpha E_c (T_s - T_i)}{3(1-\nu)} \left(1 - \frac{r}{r_s}\right) \quad (16)$$

$$\sigma_t = \frac{\alpha E_c (T_s - T_i)}{3(1-\nu)} \left(1 - 2\frac{r}{r_s}\right) \quad (17)$$

$$\sigma_z = \frac{\alpha E_c (T_s - T_i)}{1-\nu} \left(\frac{2}{3} - \frac{r}{r_s}\right) \quad (18)$$

The thermal strain on the outer surface of the cylinder is

$$\varepsilon_z(r = r_s) = \frac{\alpha(T_i - T_s)}{3} \quad (19)$$

In Eqs. (16)–(19) α is the linear coefficient of thermal expansion and T_s and T_i denote the temperatures of outer surface and in the middle of the test specimen, respectively.

5. Freezing and thawing tests

5.1. Test specimen and test arrangements

To compare the theoretical results with test results concrete cylinders having a diameter of 65 mm and height of 190 mm were produced. There was produced one test series of non air-entrained concretes (air content 1.6%) having À100-mm cube strength of 45.8 MPa and a comparison air-entrained test series (air content 5.5%) had the same compressive strength 45.8 MPa. Composition and strength results of the test concretes are presented in Table 1. The aggregates were sieved into five fractions and their petrographic composition was mostly granite. The air-entraining admixture was a vinsol resin. The chemical composition

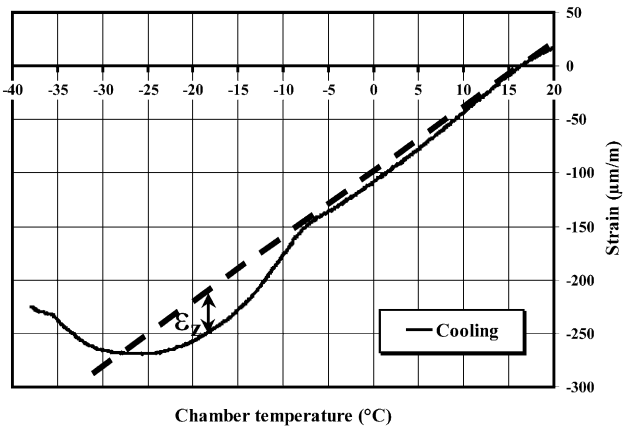

Fig. 9. The strains caused by thermal contraction were subtracted from the other cooling-induced strains by calculating the coefficient of thermal expansion from test data between +20 and +10 °C.

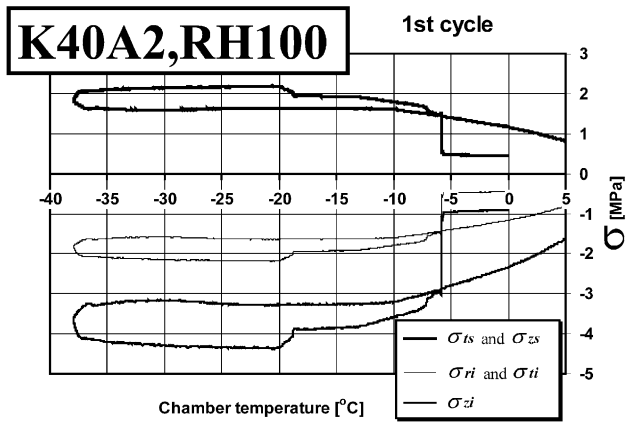

Fig. 10. Theoretical stresses in test concrete specimen K40A2,RH100 during the first cycle of the test run.

and physical properties of the rapid hardening portland cemewn in Table 2.

The test cylinders were demoulded after 24 h and half of the specimens were water cured for 28 days. The other half of the cylinders were preserved in closed containers in which the relative humidity was kept constant at 96% RH by saturated salt solution. At the age of 30 days the air-filled pore space of the cylinders was measured by a pressure test in which, after capillary suction, the specimen pore structure was filled with water in a pressure of 15 MPa for 24 h. Prior to the pressure test the cylinders were weighed in air and under water. After the pressure test, the cylinders were weighed in air. The tests were performed according to Finnish standard SFS 4475. Subsequently, cylinders were dried in an oven at a temperature of 950 °C. Pore data of the concretes are presented in Table 3.

Protective pore ratio is calculated by dividing the volume of the pore space, which is not filled by water in the capillary suction test, by the total pore volume of concrete.

Before the freezing and thawing test a hole having diameter of 10 mm and depth of 60 mm was drilled axially into the test cylinders and a relative-humidity- and temperature-measuring gauge produced by Vaisala Oy was mounted into the hole and insulated according to Fig. 2. The concrete specimens were placed into airtight separate steel cylinders having a diameter of 160 mm and height of 250 mm. Relative humidity and temperature of the steel chambers were measured by similar measuring devices as in the drilled hole in the concrete specimen.

The test specimens in the steel chambers were cooled from 20 to −38 °C with a cooling rate of 3.0 °C/h. Warming rate was 4.2 °C/h and temperature rose to +7 °C. Thereafter, cooling and warming procedure was repeated three times. In the last cycle the temperature rose to 20 °C. Before the test, two inductive strain gauges were mounted on the surface of the specimen, so that axial strain of the surface could be measured during the test run. Temperature, relative humidity, and strain data were measured

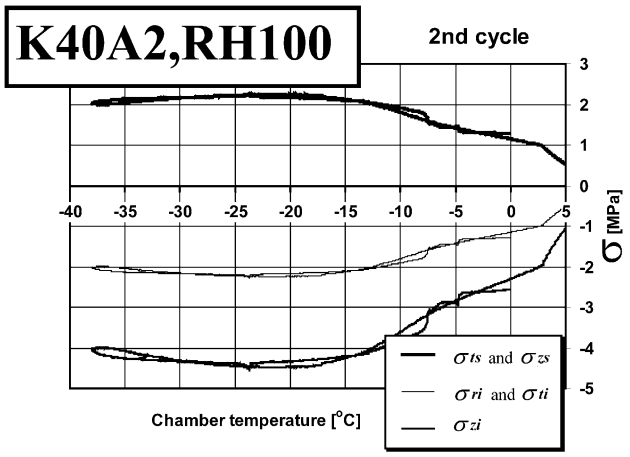

Fig. 11. Theoretical stresses in test concrete specimen K40A2,RH100 during the second cycle of the test run.

every 60 s throughout the test run and stored in a computer hard disc.

5.2. Test results

Pore size distributions of the test concretes is presented in Fig. 3 and other pore data are shown in Table 3. After the freezing and thawing tests the surface of the test specimens was observed by stereo microscope. All test cylinders had a crack pattern in which cracks were induced in the axial direction of the cylinder and perpendicularly to the axis (Fig. 4). The strain results and relative humidity results of the four test specimen groups are presented in Figs. 5–8.

6. Comparison of the test results with the theoretical results

In order to subtract the strains caused by the thermal contraction from all other strains caused by cooling and warming of the concrete cylinders a procedure presented in Fig. 9 was applied. Strain components to be studied are strains caused by pore pressure differences between the surface and inside of the cylinder before freezing, the strains caused by freezing and thawing pressures of the pore water, and the strains originating from the temperature differences between surface and middle part of the specimen. These strains denoted in Fig. 9 by ε_z were compared with the strains calculated by formulae (15) and (19). The pore water pressure values p_s and p_i in these equations were obtained by applying Eqs. (1) and (2). Concrete pressures were obtained by multiplying pore water pressures by the ratio of evaporable water volume to concrete volume V_{evap}/V_{con}.

The theoretical stresses of Eqs. (12)–(14) and Eqs. (16)–(18), which have been obtained by applying the linear theory of elasticity are presented in (Figs. 10–14). Fig. 15 presents an example of the theoretical pressures in a test concrete. The theoretical strains calculated by

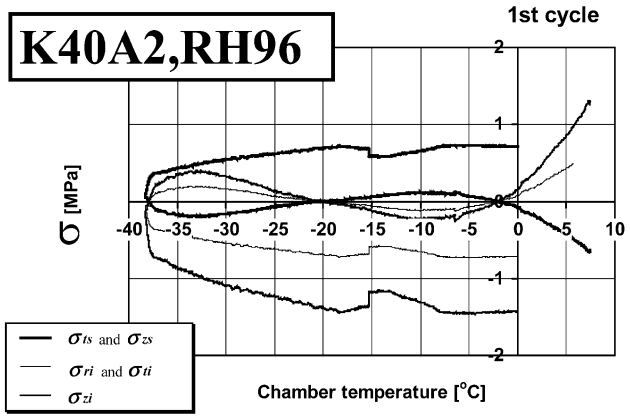

Fig. 12. Theoretical stresses in test concrete specimen K40A2,RH96 during the first cycle of the test run.

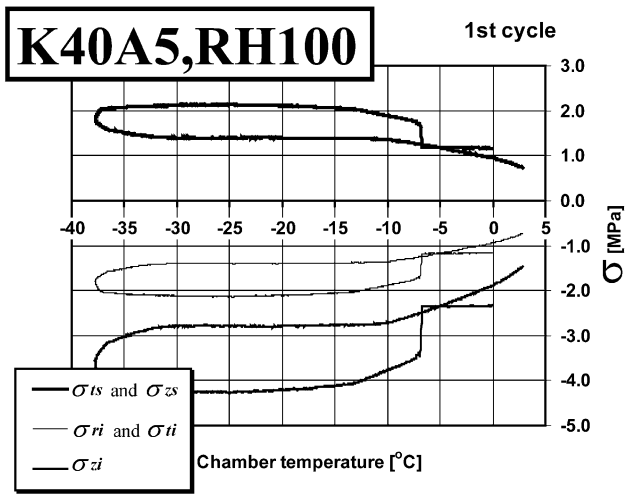

Fig. 13. Theoretical stresses in test concrete specimen K40A5,RH100 during the first cycle of the test run.

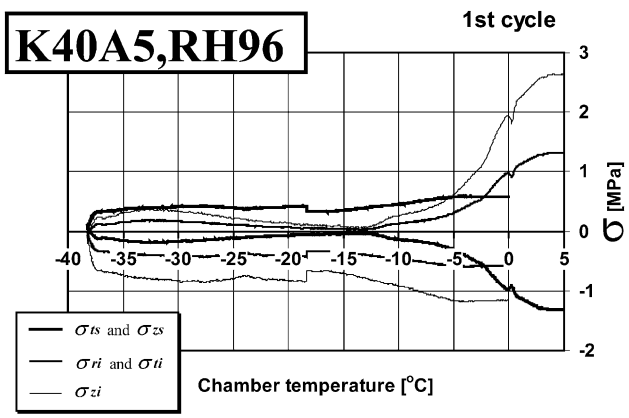

Fig. 14. Theoretical stresses in test concrete specimen K40A5,RH96 during the first cycle of the test run.

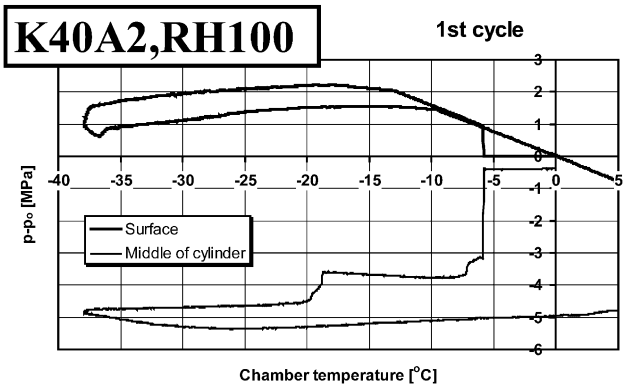

Fig. 15. Theoretical pressures in test concrete specimen K40A2,RH100 during the first cycle of the test run.

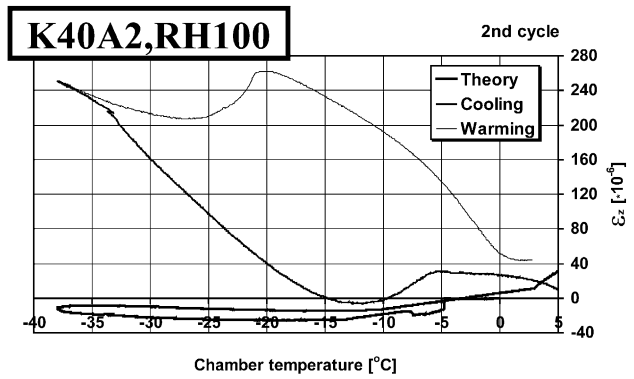

Fig. 17. Theoretical strains ε_z and test results of test concrete specimen K40A2,RH100 during the second cycle of the test run.

Eqs. (15) and (19) are compared with the test results ε_z in Figs. 16–20.

7. Discussion

The data presented in Table 3 give information on the water-filling degree of the test concretes. These data are shown also in Fig. 21. It can be noticed that in test concrete K40A2,RH100 evaporable pore water volume fills over 92% of the total pore volume while in air-entrained concrete K40A5,RH100 the respective value is only about 74%. When the test concretes have been cured in a relative humidity of 96% the pore-filling degrees are 77% in K40A2,RH96 and 61% in test concrete K40A5,RH96. The degree of pore water saturation varies quite much in the test concretes. The protective pore ratio calculated according to Finnish standard SFS 4475 shows that the non air-entrained test concrete does not fulfill the value of 0.20, which is considered to be acceptance criteria for frost resistant concrete. Air-entrained concrete K40A5 meets the requirement.

The protective pore ratio is measured after capillary suction has filled capillary pore space and, therefore, it gives information on the potential risk of freezing damage in a one-cycle freezing situation. Protective pore ratio does not take into consideration the thermodynamic pump effect that can increase the evaporable pore water amount in cyclic freezing and thawing situation when temperature fluctuates around 0 °C, for example, between −10 and +5 °C.

In comparing the strain curves presented in Figs. 5–8 it can be noticed that only in test concrete K40A2,RH100, Fig. 5, the residual dilation accumulates after every cycle due to increasing crack formation. In the other test concretes the first freezing and thawing cycle deviates from the following three. The first freezing temperature is about 5 °C lower than in the following cycles. The strain cycle of the non air-entrained test concrete K40A2,RH96, Fig. 6, is quite similar to the air-entrained test concretes.

When the relative humidity cycles of the test concretes presented in Figs. 5–8 are compared with each other the following observations can be made. In the test cylinders cured under water (K40A2,RH100 and K40A5,RH100) relative humidity measured inside the concrete is some 20 percentage units lower than in the chamber. This is the main reason for high freezing-pressure differences between the outer surface and in the middle of the specimen. This is obvious when pressure equation (2) is studied. The relative

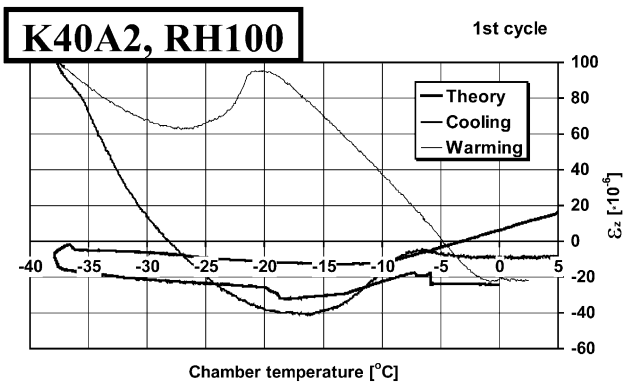

Fig. 16. Theoretical strains ε_z and test results of test concrete specimen K40A2,RH100 during the first cycle of the test run.

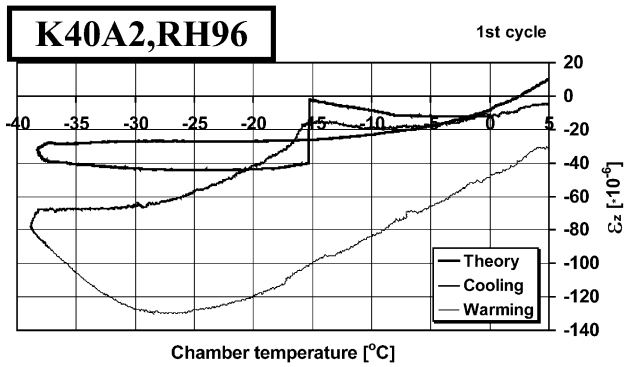

Fig. 18. Theoretical strains ε_z and test results of test concrete specimen K40A2,RH96 during the first cycle of the test run.

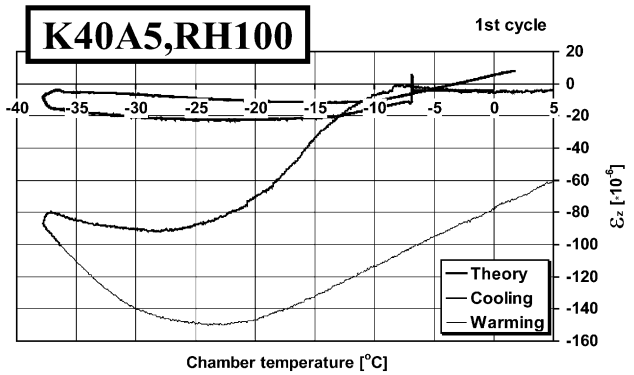

Fig. 19. Theoretical strains ε_z and test results of test concrete specimen K40A5,RH100 during the first cycle of the test run.

humidity cycles of these concretes are quite similar even though one is air-entrained and has much smaller pore-filling degree than the non air-entrained concrete K40A2,RH100.

During the end phase of the thawing cycles in temperature range from +3 to +5 °C the relative humidity of the non air-entrained test concrete K40A2,RH100, Fig. 5, drops 10 percentage units. This is a manifestation of a small thermodynamic pump effect that can increase pore water amount in every cycle if there is free moisture in vapor or liquid form in the environment. In these tests, the freezing chambers were sealed and no additional moisture could enter the chambers. The difference between relative humidity curves of concrete and chamber in test specimen K40A2,RH96, Fig. 6, was much smaller especially in the cooling phases. This means that tensional stresses will also be smaller than in the concretes preserved in 100% RH. In this test specimen the thermodynamic pump effect apparent at the end of the warming phases is somewhat more pronounced compared to test concrete K40A2,RH100.

Air-entrained test concrete K40A5,RH96 preserved in 96% RH behaved quite differently in freezing and thawing cycles. In the relative humidity curves presented in Fig. 8 it can be noticed that during the thawing phase, approximately

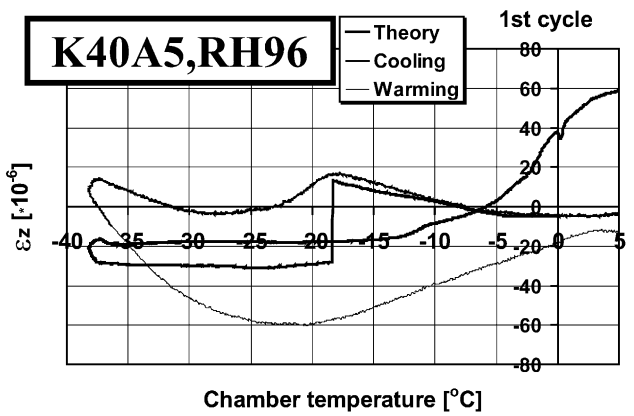

Fig. 20. Theoretical strains ε_z and test results of test concrete specimen K40A5,RH96 during the first cycle of the test run.

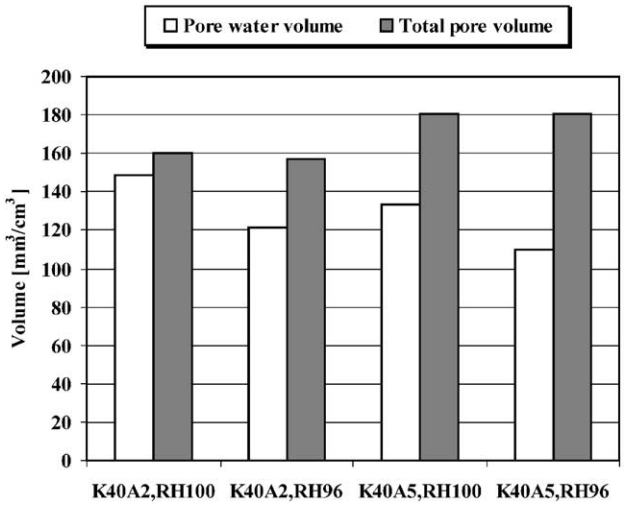

Fig. 21. Pore water volumes and total pore volumes of the test concretes.

at the temperature of −15 °C, the relative humidity in the chamber began to decrease so that around −5 °C the relative humidity in the chamber fell below that in conrete. The lowest value, 70% RH, was detected around +3 °C. This huge thermodynamic pump effect can draw up large quantities of moisture from the environment if there is moisture available. Air-entrained concretes and also non air-entrained concretes preserved in lower relative humidity behave as sponges and draw up water during every cycle increasing pore water amount, which can lead up to increased freezing damages.

The thermodynamic pump effect has a remarkable consequence on the pressure situation in the concrete and subsequently on the stress state. Pressure situation and stress state in concrete is reversed when relative humidity in the chamber goes below the relative humidity in concrete. Those parts of the cross section that are loaded with compressive stresses due to freezing pressures will become tensionally stressed and vice versa. Large tensile stresses can be expected in the center area of the cylinder specimen because of the large relative humidity drop in the chamber, at the positive temperature range of the thawing cycle of air-entrained concretes.

Sometimes the increased absorption of water into the test sample during freezing and thawing cycles is associated with the scaling and crack formation in concrete [19]. However, the results of this research project do not confirm that finding. The non air-entrained concrete that deteriorated most (K40A2,RH100) possessed only very limited relative humidity drop in the sample chamber at the end of thawing. In test concrete K40A5,RH96 the relative humidity in the test chamber decreased enormously during the end of the thawing phase but no noticeable deterioration could be seen in the strain results. Similarly, in test concrete K40A2, RH100 the residual dilation accumulates after every cycle due to increasing crack formation. If the crack formation should be the reason for the relative humidity decrease in

the test chamber, the relative humidity drop should increase with the deterioration degree. However, the relative humidity curves in Fig. 5 of every cycle lie over each other in the end part of thawing. The reason for the phenomenon is the redistribution of pore water in the pore system during freezing and thawing cycle. During freezing pore water from smaller pores is moving to the larger pores, which is caused by the differences between the chemical potential of the ice surface and the unfrozen pore water of the smaller pores situated in the vicinity of the ice surface. During thawing the pore water returns to the smaller pores causing suction into the pore system and subsequently concrete draws moisture from the surrounding environment. The theoretical basis and test results of the phenomenon have been presented in Refs. [20–22].

7.1. Pressures and stresses induced by freezing and thawing

During the subzero chamber temperatures from −4 to −9 °C of all test specimens relative humidity in the chamber was 100% and pressure on the outer surface was zero according to Eq. (1). In the middle part of concrete, the negative water pressure calculated by Kelvin's equation causes a compression state in concrete before ice is formed in the test cylinders. The first freezing temperatures of the test specimens K40A2,RH100 and K40A5,RH100 cured under water occurred at temperatures from −4 to −7 °C, Fig. 15. This causes a stepwise increase of pressure in concrete at the outer surface to the value of 1 MPa and a decrease in the negative pressure in the middle of the concrete specimen. During the subsequent cooling of the test chamber, overpressures at the surface of the cylinder increased to the values of 1.4 and 1.6 MPa in these test concretes. The underpressures in the middle of the test specimens increased to the value of 4.7 MPa in non air-entrained concrete cylinders and to the value of 4.2 MPa in air-entrained concrete specimens. During the warming phases the maximum pressures calculated by the presented theory ranged from 2 to 2.2 MPa overpressure at the surface of the cylinder and from 5.3 and 4.7 MPa underpressure, respectively.

The first freezing temperatures of test concretes K40A2,RH96 and K40A5,RH96 were −15 and −18 °C in the first cycle and −10 and −13 °C in the second cycle, respectively. When freezing takes place in these concretes and the pressure formula governing the phenomenon changes from Eq. (1) to Eq. (2) there is an abrupt jump in the pressure curves. In test concrete K40A2,RH96 the surface pressure jumps from −0.6 to 1.4 MPa, and in test concrete K40A5,RH96 surface pressure jumps from −1.2 to 1.0 MPa during the first cycle. In the real structure the pressure change is, of course, not so abrupt but more gradual.

In (Figs. 10–14 are presented the theoretical stresses induced into the test cylinders during the first freezing and thawing cycle. They are calculated by formulae (12)–(14) and (16)–(18) which are based on the linear theory of elasticity and material is assumed homogeneous and no cracks are assumed to exist. In reality, the concrete cylinders have numerous shrinkage cracks and other defects. However, the linear theory is mostly used in structures made of plain concrete.

In the test cylinders that are preserved under water (K40A2,RH100 and K40A5,RH100) freezing pressures cause a remarkable increase in the stress state and the largest tensile stresses are induced at the surface of the cylinders, Figs. 10 and 13). Stresses in the direction of the cylinder axis σ_{zs} and in the tangential direction of the surface σ_{ts} are of equal value. The largest compressive stress is in the center of the cylinder in the direction of the axis σ_{zi}. The maximum tensional and compressive stresses of the cylinders cured under water were nearly same in the non air-entrained and air-entrained concretes. The theory gave as maximum tensional stress the value 2.2 MPa and as maximum compressive stress −4.3 MPa. During the warming part of the cycle, all stresses were smaller than at the cooling stage. The stresses of the second to fourth cycles were quite similar as during the first cycle and, therefore, they are not presented in the paper.

Concrete cylinders preserved in relative humidity of 96% prior to the test had clearly smaller freezing-induced stresses compared to those cured under water with the exception of the chamber temperature range 0 to +5 °C at the end of the thawing phase, Figs. 12 and 14. In the non air-entrained concrete K40A2,RH96 maximum tensile stress σ_{zi} exceeded 1 MPa. The maximum tensile stress σ_{zi} of K40A5,RH96 exceeded 2.5 MPa at the same phase of the cycle. It is somewhat surprising that the highest tensile stress appeared in air-entrained concrete that had smaller pore filling degree than the other test concretes.

7.2. Strains induced by freezing and thawing

When the freezing-induced axial strains ε_z of the test concretes presented in Figs. 16–20 is compared to the strains calculated by the theory presented in this paper it can be noticed that they deviate from each other remarkably. After the test all test concretes had a crack pattern presented in Fig. 4 and, therefore, it is not astonishing that a theory based on linear elasticity does not predict well the strains of severely cracked test samples. The steeper strain in the compression direction of the curves right after the first freezing temperature seems to indicate that the cracks forming first have their planes parallel to the axis of the cylinder. When the ε_z curve rises in the expanding direction, cracks having their planes in the perpendicular direction to the axis of the cylinder are assumed to form.

The larger hysteresis loop of the ε_z curves compared to the ε_z curves calculated according to the presented theory displays the fact that severe cracking has occurred in the test cylinders. Cracking has taken place even though the strain curves presented in Figs. 6–8 do not show the

tendency of accumulated residual strain increase after every cycle. Cracked cylinders behave as bellows. For example, in test concretes K40A2,RH96, K40A5,RH100, and K40A5,RH96 of Figs. 18–20 the ε_z curve contracts after the minimum temperature has been reached. However, an uncracked cylinder should expand in that situation according to the linear theory of elasticity. This takes place because the temperature difference between the surface and inside of the cylinder changes sign and this closes the formed cracks having their planes in the perpendicular direction to the axis of the cylinder.

The non air-entrained test concrete K40A2,RH100 shows an exceptional strain behaviour after the minimum temperature of the chamber has been passed and the warming phase has started, Figs. 16 and 17. At the temperature range around -20 °C there takes place an additional expansion in the ε_z curve. This is caused by the differences in the coefficient of thermal expansion of ice and concrete matrix. Ice has about six times larger coefficient of thermal expansion compared to that of the concrete matrix. When moist concrete cools the ice formed in the pores contracts six times faster than the matrix. Therefore, it does not cause additional expansion with the exception of the moment when ice first freezes. During the warming phase, the situation is opposite. Ice expands six times faster than concrete matrix and if the pore system is nearly filled with water and the ice volume is large, ice does not have time to melt fast enough and it causes expansion to the concrete matrix. The presented theory based on thermodynamics does not take this kind of a situation into consideration.

8. Conclusions

1. The test results seem to validate the assumption of the critical degree of saturation of the pore system after which accumulating residual expansion takes place by every freezing and thawing cycle.

2. In all test concretes, the first freezing temperature of the first freezing and thawing cycle was lower than the first freezing temperature of the subsequent cycles.

3. At the first freezing temperature in every freezing cycle the relative humidity measured in the middle of the test specimen begins to diminish. This can be used to mark the first freezing temperature in the test sample.

4. Freezing-induced pressures can be predicted by a theory based on thermodynamics. If there are no additional salts in the pore water, the variables that govern the freezing pressures are the relative humidity of the pore system and temperature inside concrete and at the surface of the structure. Additionally, the evaporable pore water volume must be measured. If there are additional salts or other dissolved materials in the pore water, the mole fraction and activity coefficient of pore water must also be known. The larger the relative humidity difference between surface and bulk concrete is the larger freezing-induced pressures are generated into the structure.

5. The thermodynamic pumping effect at the end of the thawing phase in every cycle can increase the pore water amount remarkably if free water or moisture is available on the surface of the structure or in the environment vapor. The thermodynamic pumping effect seems to be remarkably greater and more dangerous in air-entrained concretes.

6. According to the theory based on thermodynamics and linear theory of elasticity the largest expansion pressures induced into the test concretes due to freezing were on the surface of the test cylinder. The maximum expansion pressures exceeded 2 MPa. These pressures were of the same magnitude both in non air-entrained and air-entrained concretes. The largest tensional stresses in freezing occurred on the surface of the test cylinders both in the axial and tangential direction. Also, these stresses were of the same magnitude (around 2.2 MPa) both in non air-entrained and air-entrained concretes cured under water.

7. The largest tensional stresses in the warming phase took place at the end of the thawing period when the chamber temperature was around $+5$ °C. Then the maximum tension occurred inside the concrete cylinder in the axial direction of the cylinder. This maximum tensional stress was over 2.5 MPa in the air-entrained concrete and over 1 MPa in the non air-entrained concrete when the test cylinders were preserved in 96% RH.

8. The air-entrained concretes preserved in similar environments as the comparison non air-entrained concretes had always much smaller pore-filling degrees.

9. The axial strains ε_z of the test cylinders caused by cooling and freezing-induced stresses had much larger hysteresis loops compared to strains predicted by the theory based on thermodynamics and the linear theory of elasticity. This discrepancy was caused by severe cracking that was apparent in the surface of the test cylinders after the freezing and thawing test. All test concretes cured under water or preserved in 96% RH had a rectangular crack pattern having planes parallel and perpendicular to the cylinder axis.

10. When the pore volume of non air-entrained concrete was filled 92% with water an additional expansion was detected in the thawing phase of the cycle at -20 °C.

References

[1] T.C. Powers, A working hypothesis for further studies of frost resistance of concrete, J. Am. Concr. Soc. 16 (1945) 245–271.
[2] T.C. Powers, The air requirements of frost-resistant concrete, Proceedings of the Highway Research Board, Portland Cement Association, Bulletin 33, 1949, pp. 1–28.
[3] T.C. Powers, T.L. Brownyard, Studies of the physical properties of hardened Portland cement paste, J. Am. Concr. Inst. 18 (1947) 549–602.
[4] T.C. Powers, T.L. Brownyard, Studies of the physical properties of hardened Portland cement paste, J. Am. Concr. Inst. 18 (1947) 933–969.

[5] T.C. Powers, R.A. Helmuth, Theory of volume changes in hardened Portland-cement paste during freezing, Proc. Highway Res. Board 32 (1953) 285–297.
[6] D.H. Everett, The thermodynamics of frost damage to porous solid, Trans. Faraday Soc. 57 (1961) 1541–1551.
[7] D.H. Everett, J.M. Haynes, Capillary properties of some model pore systems with special reference to frost damage, RILEM Bull. (New series) 27 (31).
[8] C.G. Litvan, Phase transitions of adsorbates: III. Heat effects and dimensional changes in nonequilibrium temperature cycles, J. Colloid Interface Sci. 38 (1) (1972) 75–83.
[9] E.W. Sidebottom, C.G. Litvan, Phase transitions of adsorbates—Vapour pressure and extension isotherms of the porous-glass + water system below 0 °C, Trans. Faraday Soc. No. 585 67 (9) (1971) 2726–2736.
[10] C.G. Litvan, Phase transitions of adsorbates: IV. Mechanism of frost action in hardened cement paste, J. Am. Ceram. Soc. 55 (1971) 38–42.
[11] C.G. Litvan, Phase transition of adsorbates: V. Aqueous sodium chloride solutions adsorbed on porous silica glass, J. Colloid Interface Sci. 45 (1973) 154–169.
[12] M.J. Setzer, Einfluß des Wassergehalts auf die Eigenschaften des erhärteten Betons, Dtsch. Aussch. Stahlbeton 280 (1977) 43–117.
[13] V. Penttala, Freezing-induced strains and pressures in wet porous materials and especially in concrete mortar, Adv. Cem. Based Mater. 7 (1998) 8–19.
[14] E.K. Attiogbe, Predicting freeze–thaw durability of concrete—a new approach, ACI Mater. J. 93 (5) (1996) 457–464.
[15] V. Penttala, Strains and pressures induced by freezing mortars exposed in sodium chloride solution, Concr. Sci. Eng. 1 (1) (1999) 2–14.
[16] M. Brun, A. Lallemand, J.-F. Quinson, C. Eyraud, A new method for the simultaneous determination of the size and shape of pores: The thermoporometry, Thermochim. Acta 21 (1977) 59–88.
[17] D.R. Lide, CRC Handbook of Chemistry and Physics, CRC Press, Boca Raton, 1991.
[18] V. Penttala, Nature of compression strength in concrete, Mag. Concr. Res. 44 (159) (1992) 87–106.
[19] S. Jacobsen, E.J. Sellevold, Frost testing high strength concrete: Scaling and cracking, Fourth International Symposium on the Utilization of High Strength/High Performance Concrete, vol. 2, 1996, pp. 597–605.
[20] R. Auberg, Zuverlässige Prüfung des Frost- und Frost-Tausalz-Widerstands von Beton mit dem CDF- und CIF-test, Mitteilungen aus dem Institut für Baufysik und Materialwissenschaft Heft 6, Shaker Verlag, Aachen, 1999, pp. 71–72.
[21] M.J. Setzer, Basis of testing the freeze–thaw resistance: Surface and internal deterioration, in: M.J. Setzer, R. Auberg (Eds.), Frost resistance of concrete, E&FN Spon, London, 1997, pp. 157–173.
[22] V. Penttala, F. Al-Neshawy, Ice formation and pore water redistribution during 2-cycle freezing and thawing of concrete mortars, in: D.J. Janssen, M.J. Setzer, M.B. Snyder (Eds.), Proceedings of the International RILEM Workshop on Frost Damage in Concrete, PRO 25, Minneapolis (2002) 115–126.